NASA Technical Memorandum 107626

GROUND VIBRATION TESTS OF A HIGH FIDELITY TRUSS FOR VERIFICATION OF ON ORBIT DAMAGE LOCATION TECHNIQUES

Thomas A. L. Kashangaki

May 1992

NASA
National Aeronautics and
Space Administration

Langley Research Center
Hampton, Virginia 23665

ABSTRACT

This paper describes a series of modal tests that were performed on a cantilevered truss structure. The goal of the tests was to assemble a large database of high quality modal test data for use in verification of proposed methods for on orbit model verification and damage detection in flexible truss structures. A description of the hardware is provided along with details of the experimental setup and procedures for sixteen damage cases. Results from selected cases are presented and discussed. Differences between ground vibration testing and on orbit modal testing are also described.

INTRODUCTION

Future structures in space will be orders of magnitude larger and more complex than their predecessors. Structures such as the Space Station Freedom will typically be built around a large flexible frame and consist of truss members, habitat and experimental modules, flexible and articulating appendages, along with numerous utility trays and moving parts. The complexity and size of these structures, along with the need to design the spacecraft to be lightweight, strong and modular for ease of expansion, repair and modification, all require that the integrity of the structures be monitored periodically.

Several researchers [References 1, 2, 3 and 4] have proposed methods of detecting damage to large space trusses and locating the site of this damage based on changes in the vibration frequencies and modes of the structure. A research program underway at the NASA Langley Research Center is using a hybrid-scale model of the Space Station as a test-bed for studying the dynamic behavior of such structures. As part of this program, researchers are studying the implementation of an on-orbit damage location scheme. Results to date indicate that it may be possible to use the reaction control systems of the space station to perform an on-orbit modal test of the structure and extract frequency and mode shape data which might be used in this damage location technique.

In the past, damage location research has focused primarily on algorithm development and verification using analytical models and simulated test data. Although often geared towards large flexible space structures such as Space Station Freedom, researchers have used simple structures to demonstrate and validate new algorithms and techniques. The most common verification models have been multiple spring-mass models. In order to

demonstrate the robustness of their algorithms, researchers have attempted to simulate measured modes and frequencies by adding a random error to the analytical mode shapes. Very few researchers have reported using experimentally measured modal data in their model updating and damage location methods. Smith and McGowan [5] were the first to report comprehensive tests conducted specifically with damage location in mind. The tests they performed were on a "generic" truss structure using off the shelf hardware. Because of the low fidelity in the strut manufacturing, the tests were only partially successful. Other researchers have reported successful modification of finite element models based on experimentally acquired data, but to date no comprehensive tests have been performed specifically for studying damage location.

In order to fill this significant gap and provide researchers with a reliable and comprehensive database of measured data, a damage location test bed has been developed at the NASA Langley Research Center. In this paper the focus structure will be discussed, and the design and implementation of the test program will be described.

EIGHT BAY TRUSS TEST BED.

Dynamic Scale Model Technology Program

The Dynamic Scale Model Technology (DSMT) research program at the NASA Langley Research Center has the objective of developing scale model technology for verifying the dynamic analysis methods for predicting the on-orbit response of large space structures. To meet these goals DSMT has developed a hybrid scaled model of the proposed Space Station Freedom (SSF). Hybrid scaling refers to the scaling method, where the inertial properties of the components (the masses, and mass moments of inertia) have been scaled down to 1/5th the full scale model, while the overall dimensions have been scaled down to 1/10th full scale. This mixture of scaling results in a model that has five times the frequencies, and is small enough to fit in a reasonably sized laboratory. Several launch configurations of the proposed Space Station will be studied to understand the global dynamics of each of the configurations, as well as to explore the modeling requirements and the ability to predict the behavior of the fully assembled station when on-orbit. Figure 1 shows the HMB-2 test configuration which simulates the second stage of assembly of the proposed Space Station. The complexity of the

structure is evidenced by several large appendages such as solar arrays and radiators, and the rigid pallets attached to the truss.

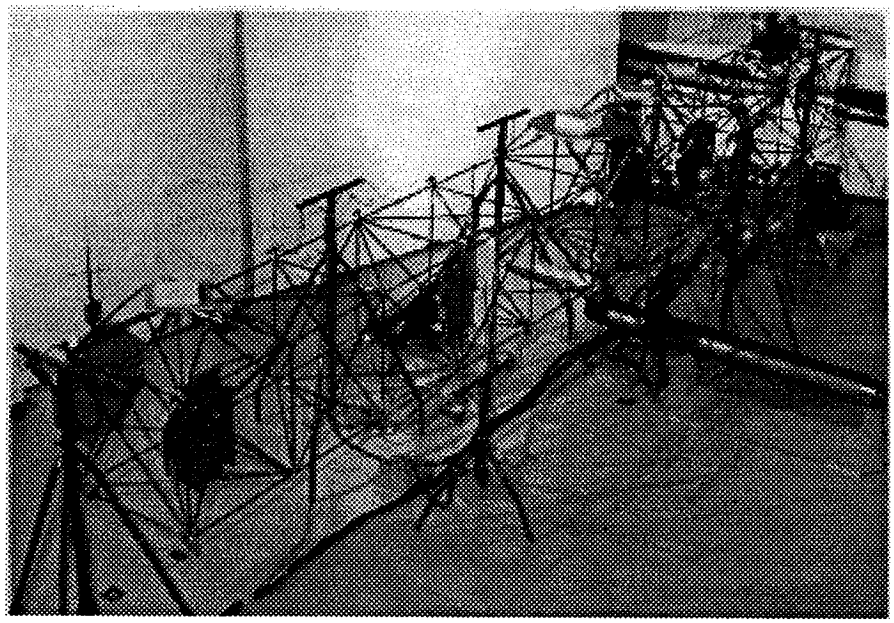

Figure 1 HMB-2 structure

Eight Bay Truss Damage Location Test Bed

As shown in Figure 2, the test article consists of eight cubic bays of the hybrid model truss structure cantilevered from a rigid backstop plate. The number of bays was selected to correspond with the largest truss section on the HMB-2 configuration of the DSMT hardware, as this was the first Space Station configuration to undergo integrated testing. Each bay consists of two different strut lengths, the longerons and diagonals, and interchangeable node ball joints. The bay size is 19.685 inches (0.5 m). The strut design characteristics are shown in Table 1. Figure 3 is a finite element model of the eight bay truss lacing pattern with definitions that will be used throughout the remainder of this work. Figure 4 is a front view of the test article, showing several accelerometers and the instrumentation wiring. Figure 5 is a cut-away view of a joint with three incoming struts, the joint-assemblies and the node-ball.

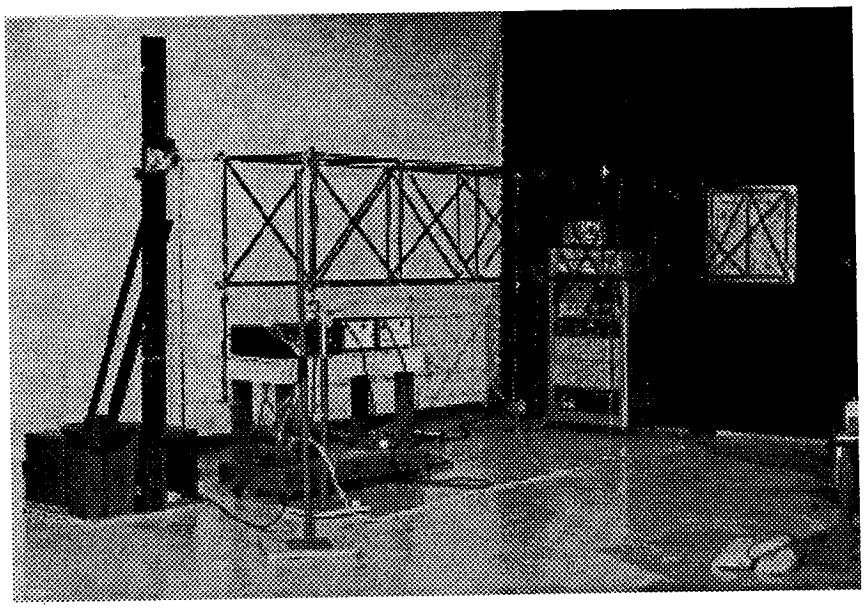

Figure 2 Eight bay test structure

Table 1 Strut Design Data

	longeron	Diagonal
Strut Length	19.685 in	27.839 in
Strut Stiffness $(EA/L)_{eff}$	13,040 lb/in	9,013 lb/in
Strut EA_{eff}	225,669 lbs	250,913 lbs
Pin-Pin Buckling Load P_{cr}	109.2 lbs	56 lbs
2 x P_{cr} Nominal Buckling Load	218.4 lbs	109.2 lbs

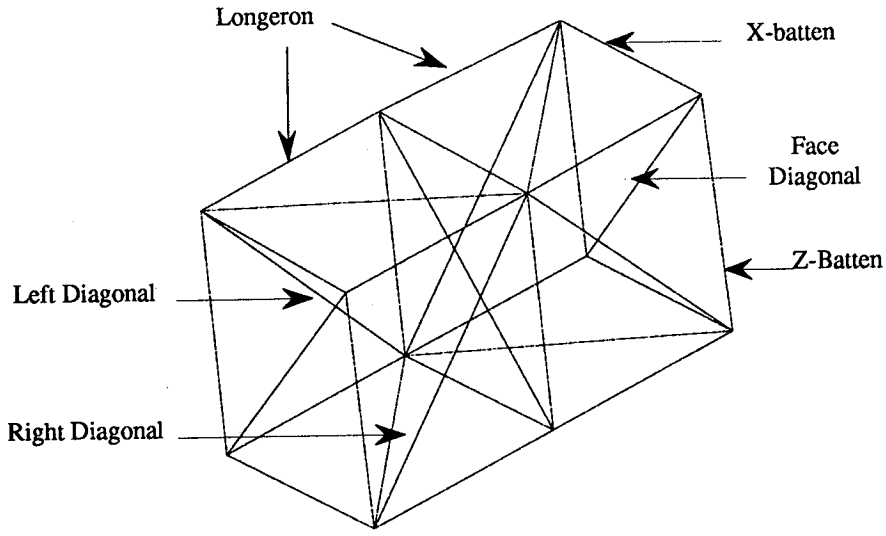

Figure 3 Eight bay truss lacing pattern

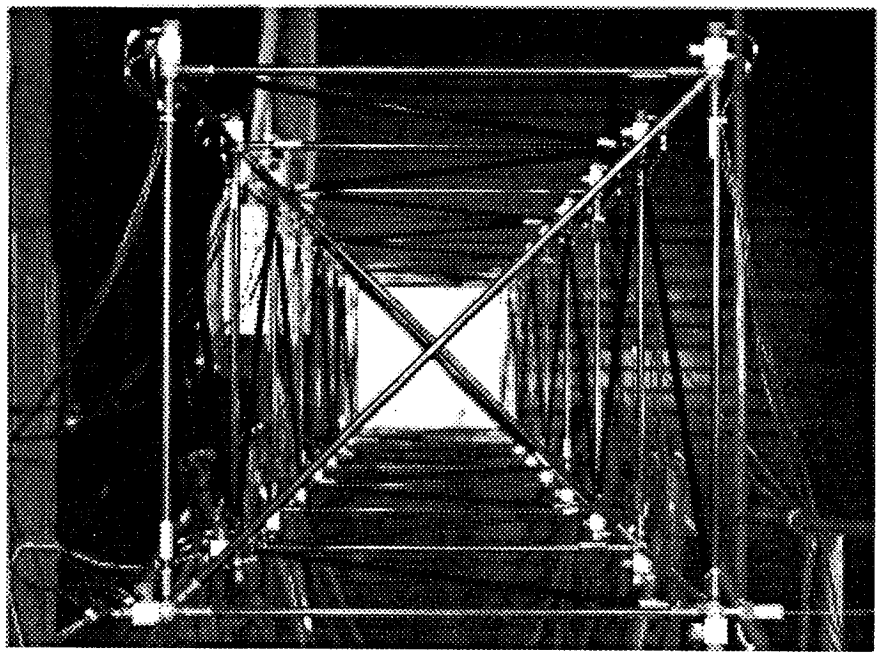

Figure 4 Eight bay truss front view

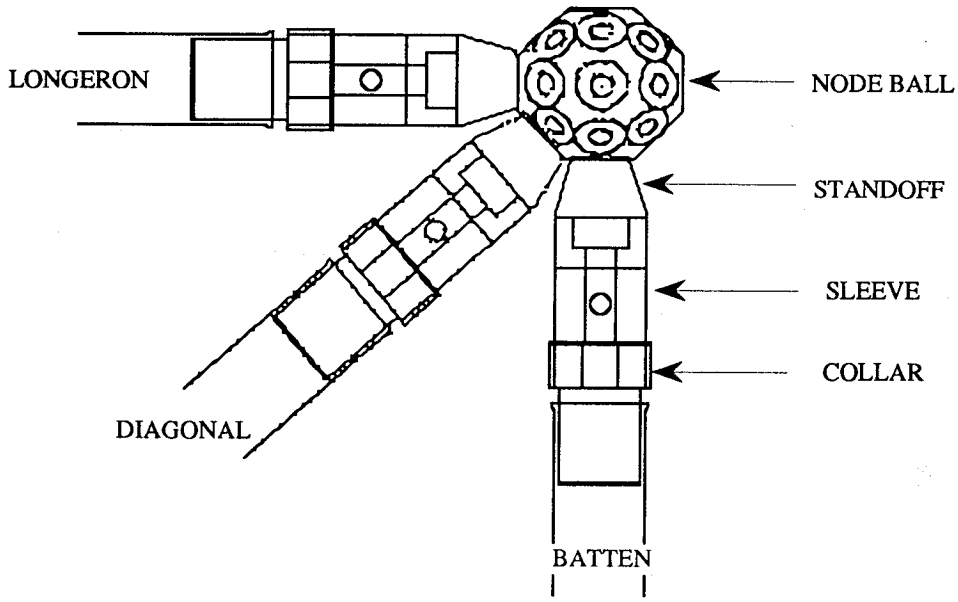

Figure 5 DSMT joint assembly and node ball configuration

MODAL ANALYSIS AND TESTING.

Introduction

This section covers the basic theory of modal analysis and modal testing. It has been summarized from a number of sources and has been included here for completeness. There are two approaches to obtaining and studying the modal response of a structure. The first of these is from mathematical models of the structure, and the second is from experimental modal analysis. Both of these approaches will be discussed here briefly., prior to a description of the tests that were performed.

In the first approach to modal analysis, mathematical models discretize a structure by breaking it into numerous springs and masses which lend themselves well to simple analysis. This process is typically performed by a finite element processor such as MSC/NASTRAN™ [6] and SDRC I-DEAS™ [7]. The eigenvalue equation is then solved using the multiple spring-mass representation and the normal modes and frequencies of the complicated system are obtained. These modes can then be used in a forced response analysis to examine the response of the system to a variety of inputs. One very important forced response analysis is to input a unit force of varying frequency at one node, while monitoring the response as a function of frequency at several important locations. This response per unit force versus frequency is called the Frequency Response Function (FRF) or transfer function.

Experimental modal analysis, on the other hand, starts out with the unit forced response data (i.e. the FRFs) and extracts the modes of vibration directly from the FRFs without having to make any assumptions about the mass and stiffness distribution. The experimental modal analysis ends with a set of modes defined by frequency, damping, mode shape coefficient and residue. Certain assumptions and post-processing of the data are necessary to calculate modal mass and stiffness, with even further assumptions and post-processing necessary to obtain physical stiffness or mass representations.

Modal Analysis Theory

Normal Modes Analysis

The equations of motion for an n degree of freedom structural dynamic system can be expressed in finite element matrix notation as :

$$[M]\{\ddot{x}\}+[D]\{\dot{x}\}+[K]\{x\}=\{f(t)\} \tag{1}$$

where

$[M]$	=	$n \times n$ system mass matrix
$[D]$	=	$n \times n$ system damping matrix
$[K]$	=	$n \times n$ system stiffness matrix
$\{x\}$	=	$n \times 1$ vector of physical displacements
$\{f(t)\}$	=	$n \times 1$ vector containing the applied loads.

The mass and stiffness matrices are both symmetric and positive definite for rigidly constrained structures. The undamped eigenvalue equation associated with equation (1) is

$$([K]-\lambda_i[M])\{\phi\}_i=0 \tag{2}$$

where λ_i ,the eigenvalue, is equal to the square of the natural frequencies of the structure. The non-trivial solution to equation (2) requires that the determinant of the coefficient matrix is equal to zero:

$$\det([K]-\lambda_i[M])=0 \tag{3}$$

This determinant is an n^{th} order polynomial whose roots are the eigenvalues, λ_i, of the structure. Each of these eigenvalues can be substituted back into equation (2) to solve for the corresponding mode shape vector $\{\phi\}_i$. The complete solution to the normal modes analysis can be expressed as two n x n matrices:

$$\left[\lambda_i\right] \text{ and } \left[\Phi\right] \tag{4}$$

where

$\lambda_i=\omega_i^2$	=	square of the i^{th} natural frequency
$\{\phi\}_i$	=	vector of mode shape coefficients at each Degree of Freedom (DOF) for mode i.

The diagonal matrix of eigenvalues is unique for each structure. The matrix of mode shape vectors, however, is subject to an arbitrary scaling factor which does not affect the shape of the mode, only its amplitude. If the mode shapes are mass-normalized then they have the following properties:

$$[\Phi]^T[M][\Phi]=[I]$$
$$[\Phi]^T[K][\Phi]=[\lambda] \tag{5}$$

Proofs and more rigorous derivations of these equations abound in the literature.

Modal Response Analysis

If the structure is excited sinusoidally by a set of forces all at the same frequency, ω, but each force having a different amplitude and phase, then

$$\{f(t)\}=\{f\}e^{i\omega t} \tag{6}$$

If we assume that a solution exists of the form

$$\{x(t)\}=\{x\}e^{i\omega t} \tag{7}$$

then the equation of motion becomes

$$\left([K]-\omega_i^2[M]\right)\{x\}e^{i\omega t}=\{f\}e^{i\omega t} \tag{8}$$

Rearranging, and solving for the response of the structure to the uncorrelated inputs results in

$$\{x\}=\frac{1}{\left([K]-\omega_i^2[M]\right)}\{f\} \tag{9}$$

which can be expressed as

$$\{x\}=[\alpha(\omega)]\{f\} \tag{10}$$

where $[\alpha(\omega)]$ is the n x n receptance matrix for the structure. Each element of the receptance matrix is a frequency response function describing the response at DOF i to the unit input at DOF j while all other inputs are assumed equal to zero. Therefore, each FRF can be expressed as:

$$\alpha_{jk}(\omega)=\left(\frac{x_j}{f_k}\right)_{f_m=0;\,(m=1,2,..n;\neq k)} \tag{11}$$

If measurements of the response of the structure at all n DOF for each excitation can be made, the full receptance matrix is an n x n symmetric matrix of the form shown in Figure 6.

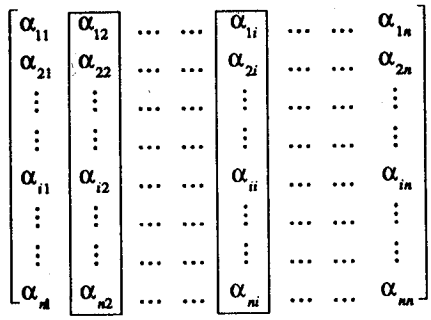

Figure 6 Typical receptance matrix with two excitations highlighted

In a typical test, only a few excitation sources are used. In the tests described in the following sections, for example, only two shakers are used to excite the structure. Each column of the receptance matrix represents the full response of the structure to one excitation source. Therefore, as highlighted in Figure 6, a two shaker test provides two columns of the receptance matrix. In addition, in most tests, not all DOF are instrumented with sensors, resulting in incomplete columns of the matrix being filled. In order to derive the modal properties (frequencies, damping and mode shapes) for a structure with *r* instrumented DOF from experimentally acquired FRFs, at least *r* entries from one column need to be measured, including the "Driving Point" FRF. This is the FRF for the DOF at which the excitation is applied. Ewins [8] reports that this is the minimum number of FRFs that are needed to derive a modal model. Typically, additional data is acquired to ensure that the modal data is accurate.

Turning to the individual frequency response function itself, equation (8) can be expressed as

$$\left([K]-\omega^2[M]\right)=[\alpha(\omega)]^{-1} \tag{12}$$

Pre- and post-multiplying each side of this equation by the mode shapes results in

$$[\Phi]^T\left([K]-\omega^2[M]\right)[\Phi]=[\Phi]^T[\alpha(\omega)]^{-1}[\Phi] \tag{13}$$

Expanding, and simplifying with the orthogonality relationships

$$[\Phi]^T[K][\Phi]-\omega^2[\Phi]^T[M][\Phi]=[\Phi]^T[\alpha(\omega)]^{-1}[\Phi] \tag{14}$$

or

$$\lambda_i-\omega^2=[\Phi]^T[\alpha(\omega)]^{-1}[\Phi] \tag{15}$$

The receptance matrix can then be expressed as

$$[\alpha(\omega)]=[\Phi]\left[\lambda_i-\omega^2\right]^{-1}[\Phi]^T \tag{16}$$

which is simpler to compute than the formulation in equation (11). Notice that the individual FRF can now be computed as

$$\alpha_{ij}(\omega)=\sum_{i=1}^{n}\frac{\left({}_i\phi_j\right)\left({}_i\phi_k\right)}{\lambda_i-\omega^2}=\sum_{i=1}^{n}\frac{{}_iA_{jk}}{\lambda_i-\omega^2}=\frac{x_j}{f_k} \tag{17}$$

where

$\left({}_i\phi_j\right)$ = the mode shape coefficient for mode i at DOF j

${}_iA_{jk}$ = the modal constant or residue

Notice that, if the structure is vibrating at one of the natural frequencies (i.e., $\omega^2 = \lambda_i$), the denominator of equation (17) goes to zero and, for an undamped structure, the FRF goes to infinity. In lightly damped structures, the resonance shows up as a peak on the FRF curve.

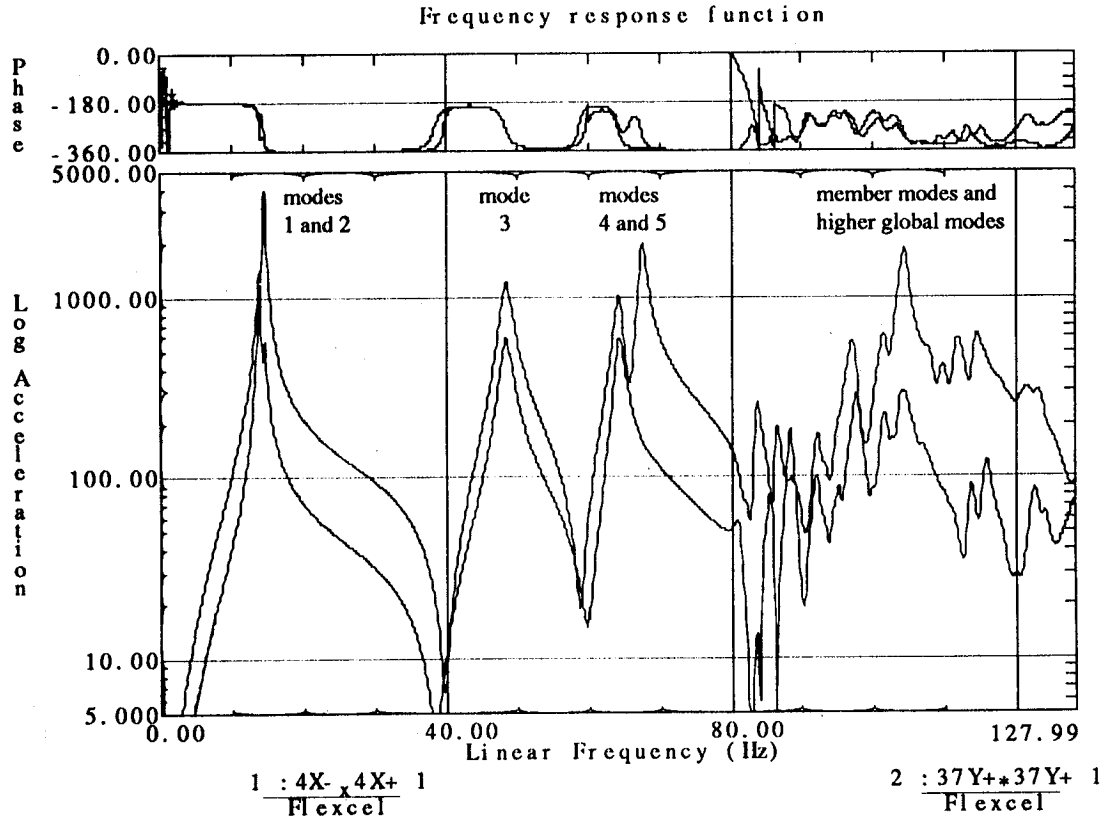

Figure 7 Driving point FRF for undamaged eight bay truss

Figure 7 shows the two driving point frequency response functions from tests of the undamaged eight bay truss. Notice that the first two modes are very close together, but the two FRFs are able to distinguish the modes. The third mode is a torsional mode and the fourth and fifth modes are the second bending mode pair. Above 80 Hz. the individual diagonals and longerons begin to vibrate and the next global mode is not easily discernible among the member modes. As described in the next section, this results in only the first five modes being available for damage location. Notice, also, that the phase is also plotted. At each resonance there is a change of phase, and likewise at each anti-resonance.

FINITE ELEMENT ANALYSIS

Introduction

In the previous section the finite element equations were derived for an n x n structural system. In this section, application of the Finite Element Method (FEM) dynamic analysis will be applied to the test article. The eight bay truss was modeled in the I-DEAS pre-processor SUPERTAB™, supplied by the Structural Dynamics Research Corporation (SDRC). The SUPERTAB™ translator was then used to write an input file for MSC/NASTRAN™ and a normal modes analysis was performed. As part of the NASTRAN run the mass and stiffness matrices were output to MATLAB™ [9] readable files for use in sensitivity studies and for the damage location tests. The finite element modeling and normal modes results will be presented in this section as a precursor to the description of the test configuration and results.

Modeling.

SDRC I-DEAS™ was used to model each of the struts and node balls for the eight bay truss. There are 36 nodes in the truss, resulting in a system with 216 translational and rotational DOF. The full FEM mass and stiffness matrices are thus 216 x 216 in size. Because accelerometers only measure translational motion, it is common practice to reduce the FEM model to include only the x, y and z translational DOF. This was done for the eight bay truss, resulting in matrices of dimension 108 x 108. The four nodes cantilevered to the wall were assumed rigidly fixed, thus removing an additional 12 DOF from the model. The final analysis model thus contains matrices of dimension 96 x 96.

The struts were modeled as NASTRAN CBAR elements, each with three translational DOF at each node. Half of the mass of each beam was lumped at the two nodes connecting the beam element. Lumped mass elements were used to model the node balls and the accelerometers. In addition, a lumped mass value was added for the accelerometer and a percentage of the cable masses, even though an attempt was made to off load as much of the cable mass as possible in the test. The added stiffness of the accelerometer cables was considered negligible.

The final model contained a total of 109 CBAR elements and 108 lumped masses. A summary of the element masses is provided in Table 2. The element material and physical properties were derived from tests of the individual members, along with information provided by the manufacturer.

Table 2 Eight Bay FEM Mass Summary

	Mass (grams)	Mass (pounds)	Number in 8 Bay Truss	eightbay totals (pounds)
node ball	5.85	0.0128	36	2.6935
longeron	28.75	0.0396	68	2.4524
diagonal	37.33	0.0598	41	0.4608
joint assembly	7.62	0.0170	218	3.7001
Triax + Block	11.0	0.0243	32	0.776
		TOTAL		10.0776

Normal Modes Analysis

A NASTRAN normal modes analysis (solution 63) was performed to find the first ten global modes and frequencies for the undamaged eight bay truss structure. Of the first ten global modes, the first is a bending mode, as is the second. The third mode is the first torsion mode. Modes four and five are the second bending pair. Mode six is the first axial mode. In a typical test, only the first few modes of a structure can be measured accurately. It was therefore considered fortunate that one of each kind of mode was available in the first six modes. These modes (i.e. modes one through six) were targeted for measurement as described in the following sections. Table 3 describes the first six modes and frequencies for the undamaged eight bay structure. Figure 8 shows these first six modes. For a symmetric cantilevered beam, the first two modes are usually orthogonal bending modes of the same frequency. The fourth and fifth modes for a symmetric cantilevered beam are also a bending mode pair with the same frequency. In this case, however, the truss is not exactly symmetric due to the lacing pattern of the

struts coming out of the wall. This is the reason for the small difference in the first two frequencies, and, for higher modes, the difference becomes even larger.

Table 3 Eight Bay Normal Modes One Through Six

MODE	FREQUENCY (HZ)	DESCRIPTION
1	14.005	First Y-X Bending
2	14.521	First Y-Z Bending
3	46.615	First Torsional
4	66.238	Second Y-X Bending
5	71.328	Second Y-Z Bending
6	117.949	First Axial

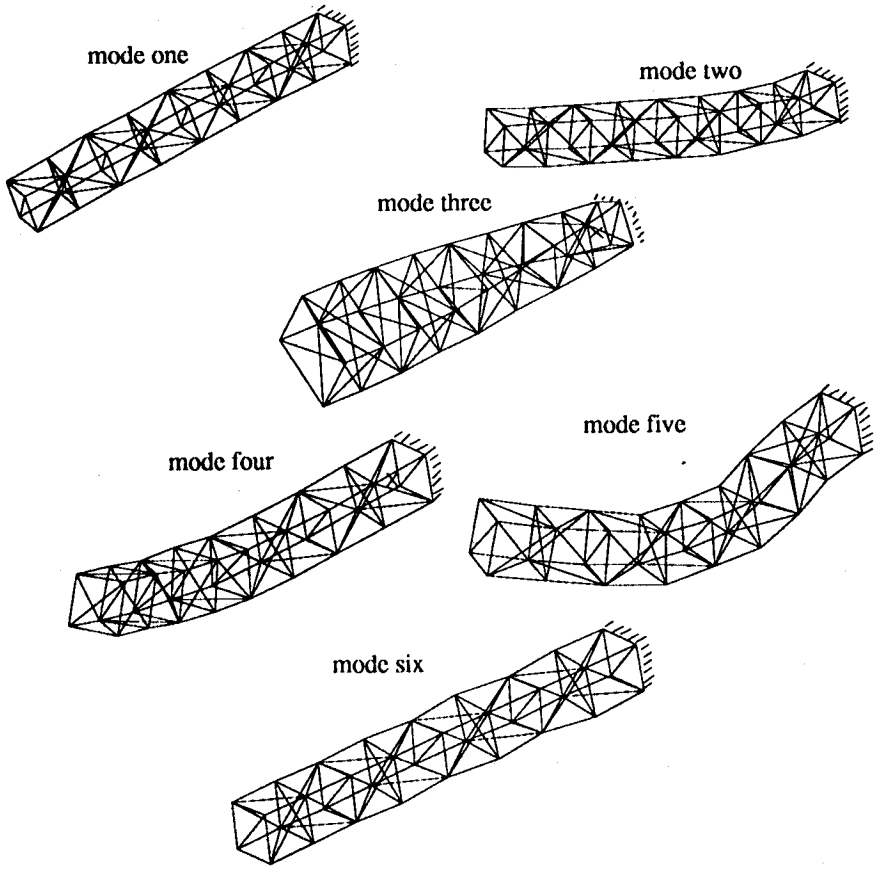

Figure 8 Eight bay normal modes one through six

The principal axes of vibration are not aligned with the global x-y-z axes, again due to the lacing pattern. As shown in Figure 9 the truss vibrates about a set of axes rotated 45°

from the global axes. Mode one is bending about the principal X axes, while mode two is bending about the principal Z axes. The same is true of the higher bending modes.

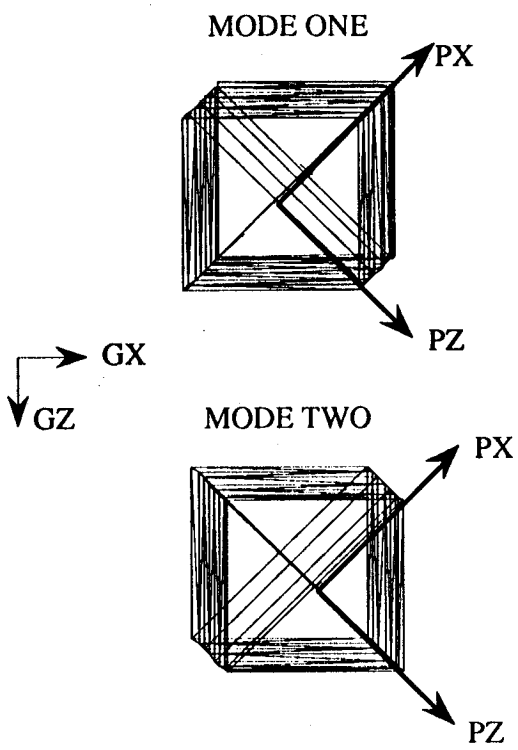

Figure 9 Global and principal axes of vibration

SELECTION AND DESCRIPTION OF DAMAGE CASES

Sixteen damage cases were selected as representative examples of the robustness of the methods and analyses presented in this work. In most cases *damage* refers to the full removal of one strut from the eight bay truss. The design of the node ball and joints for the DSMT structure make it very simple to remove and replace individual struts. This is, in part, to mimic the ease of assembly for the full scale Space Station, and also to allow for changes in the Space Station configuration as the design evolves. In addition to the 14 single member damage cases, several atypical damage cases were examined. These include a partial damage case in which a strut that had buckled during static testing of the structure was inserted in place of a normal longeron. The stiffness, or load carrying ability, of such a buckled member was assumed to have been reduced. Finally, one case of multiple struts missing was examined. Figure 10 identifies each of the struts that were involved in one of the damage cases and Table 4 summarizes the damage cases

selected, the element affected, and the bay in the truss where the element is located. Table 5 and Figure 11 show the frequency variation for the sixteen damage cases.

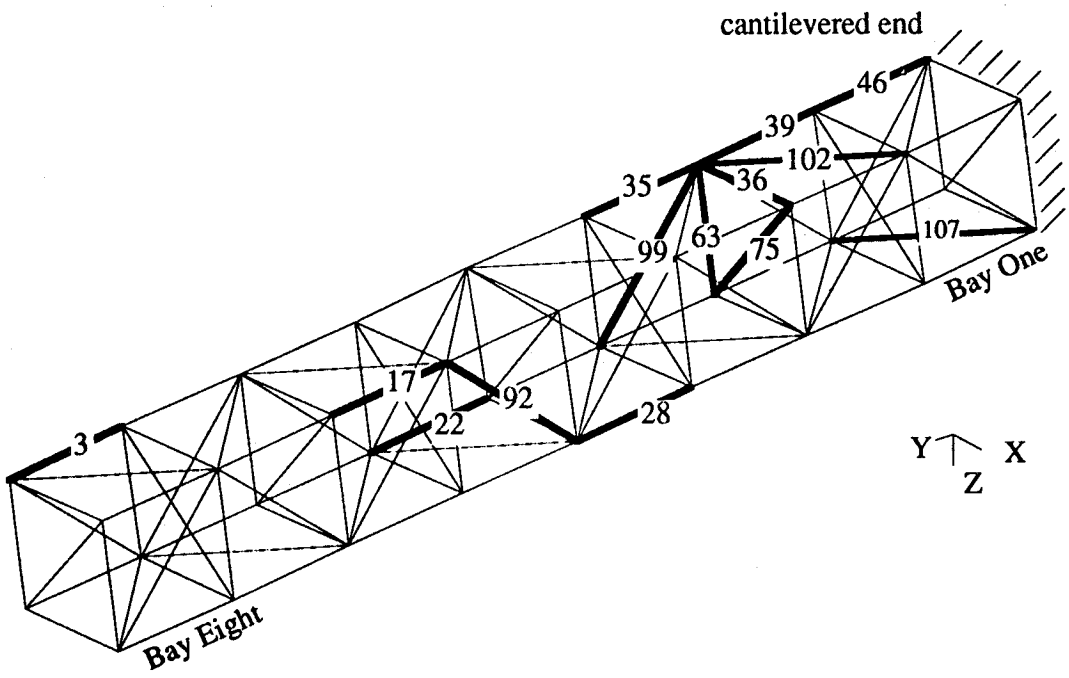

Figure 10 Eight bay damage cases

Table 4 Eight bay damage Case Definitions

DAMAGE CASE	ELEMENT LABEL	ELEMENT TYPE	BAY	NODE 1	NODE 2
A	46	LONGERON	1	29	33
B	107	LOWER DIAG	1	31	36
C	39	LONGERON	2	25	29
D	102	UPPER DIAG	2	25	30
E	36	X-BATTEN	3	25	26
F	75	FACE DIAG	3	26	27
G	63	Z-BATTEN	3	25	27
H	35	LONGERON	3	21	25
I	99	LEFT DIAG	3	23	25
J	28	LONGERON	4	20	24
K	92	RIGHT DIAG	5	14	20
L	22	LONGERON	5	15	19
M	17	LONGERON	6	10	14
N	3	LONGERON	8	1	5
O *	35 AND 99	LONGERON & DIAGONAL	3	21/23	25
P **	35	LONGERON	3	22	26

** Multiple member damage case*
*** Buckled member - Partial damage case*

Table 5 Damage Case Frequencies (Finite Element Solution)

DAMAGE CASE	MODE 1	MODE 2	MODE 3	MODE 4	MODE 5	MODE 6
NO DAM	14.01	14.52	46.62	66.24	71.33	117.95
A	9.47	14.00	46.61	66.25	68.61	108.42
B	14.63	14.36	35.88	59.94	69.16	110.50
C	9.48	14.01	46.63	66.31	68.77	109.16
D	14.36	14.33	34.77	60.63	69.16	117.02
E	14.01	14.52	46.63	66.26	71.33	114.52
F	14.01	14.52	46.65	66.42	71.46	115.37
G	14.01	14.52	46.63	66.26	71.33	114.52
H	11.42	14.01	46.65	61.40	66.38	107.38
I	14.37	14.33	35.09	64.11	69.47	117.35
J	11.43	14.01	46.67	61.54	66.43	109.14
K	14.62	14.37	39.03	66.33	71.56	95.25
L	12.36	14.54	46.70	50.67	71.51	111.63
M	14.82	14.55	46.73	54.89	71.41	102.81
N	14.07	14.56	46.76	66.37	67.71	114.73
O	9.77	13.65	34.68	59.66	64.32	102.90
P	No analysis performed because extent of damage unknown					

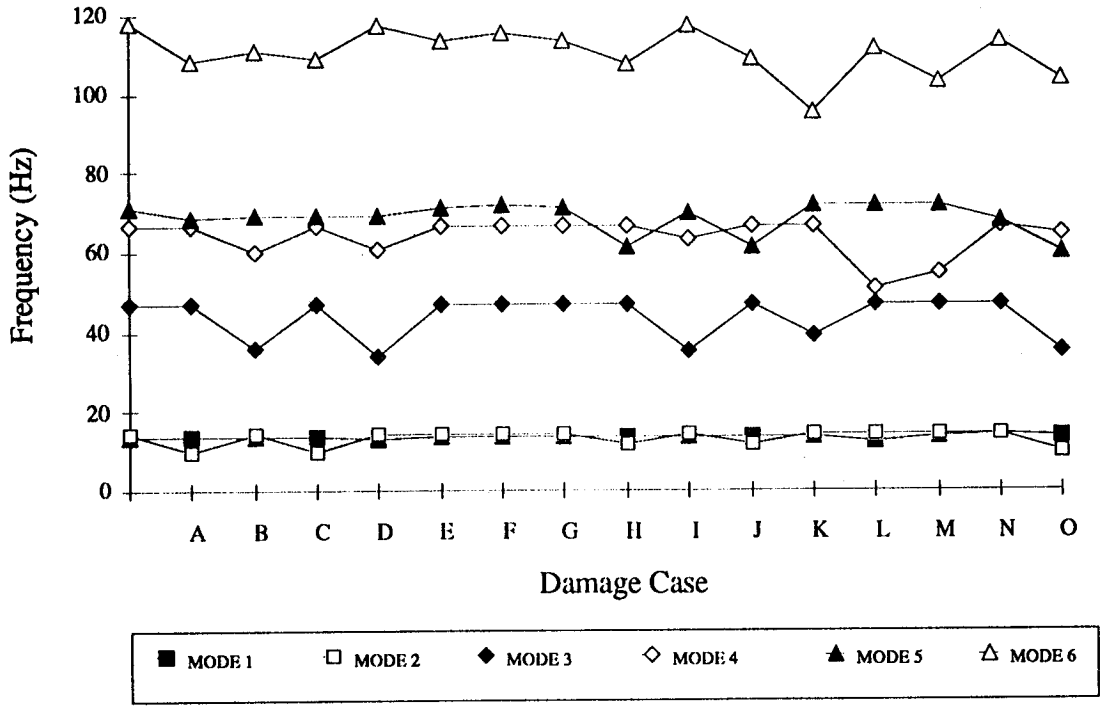

Figure 11 Frequency variations for eight bay damage cases.

EXPERIMENTAL SETUP AND RESULTS

Introduction

Although the tests in this study were performed in a laboratory on the ground, the results of this work are intended for application to orbiting structures which are unconstrained at the boundaries. These structures are not influenced by gravity and exhibit true free-free vibration. It is difficult to duplicate these conditions in a laboratory on the ground but significant steps have been taken towards simulating free-free motion using advanced suspension devices. For the purposes of damage location studies, however, the boundary conditions are not significant because the mathematical formulations take into account the end conditions. This allows the use of a cantilevered truss to study model updating and damage location techniques with great confidence that the results will translate well to a free-free structure. Figure 2 shows the cantilevered eight bay truss test configuration. The experimental setup and procedures are discussed in this section. Where there are differences between ground testing procedures and those that would be used on orbit, these are pointed out.

Over the course of this research, several test configurations were used. Each series of tests differed from the others in the number, the type and the location of the sensors and excitation sources. The results that are reported here are from a series of tests in which a total of 97 accelerometers and two shakers were employed. Results from the other tests have been reported in conference papers and NASA technical reports [10] and [11]. Table 6 lists five of the test configurations that were used during the course of this research effort. Tests with 14 and 32 accelerometers were used to study optimal sensor and excitation placement as well as mode selection. The results from the EB97-A tests, using two shakers, will be stressed. The data from this series of tests proved to be the most accurate and were the most comprehensive. This series of test data has now been made available to the research community for use in the development of model updating and damage location methods. It is anticipated that this structure and the test data will become a benchmark for evaluation of new methods and algorithms.

Table 6 Eight Bay Tests

TEST LABEL	NUMBER OF ACCELS	NUMBER OF EXCITERS	TYPE OF EXCITATION
EB14-I	14	1	IMPACT
EB14-A	14	2	BURST
EB32-A	32	2	BURST
EB32-B	32	3	BURST
EB97-A	97	2	BURST
EB97-B	97	3	BURST

Ninety-Seven Accelerometer Test Setup.

The results that are reported here are from a series of tests in which a total of 97 accelerometers were used to measure the acceleration time histories of the truss during modal testing. Two electromagnetic shakers were used as sources of excitation. In the following paragraphs, details about the sensor and shaker placement, along with other specifics about the test configuration, will be presented.

Excitation Placement

Two electromagnetic shakers were used in the EB97-A tests. The shakers selected were APS Dynamics brand with a ± 3 inch stroke. The first shaker was connected at node four in the negative x direction. The second shaker was placed at node 7 at a 45° angle such that there would be a component of the force in the positive y direction and a component in the negative z direction. This allowed for excitation of both the torsional modes and the axial mode, as well as enhancing the bending mode excitation.

The shakers were connected to the structure through 10 inch long, 0.1 inch diameter stingers as shown in Figure 12. Each stinger was attached to a PCB model 208-AO2 load cell, which was used to measure the force that was applied to the structure. Uncorrelated burst random input of about ±0.5 lb maximum force was used in each of the tests reported here. The burst random signal was generated and controlled by the signal generation capability in the data acquisition system.

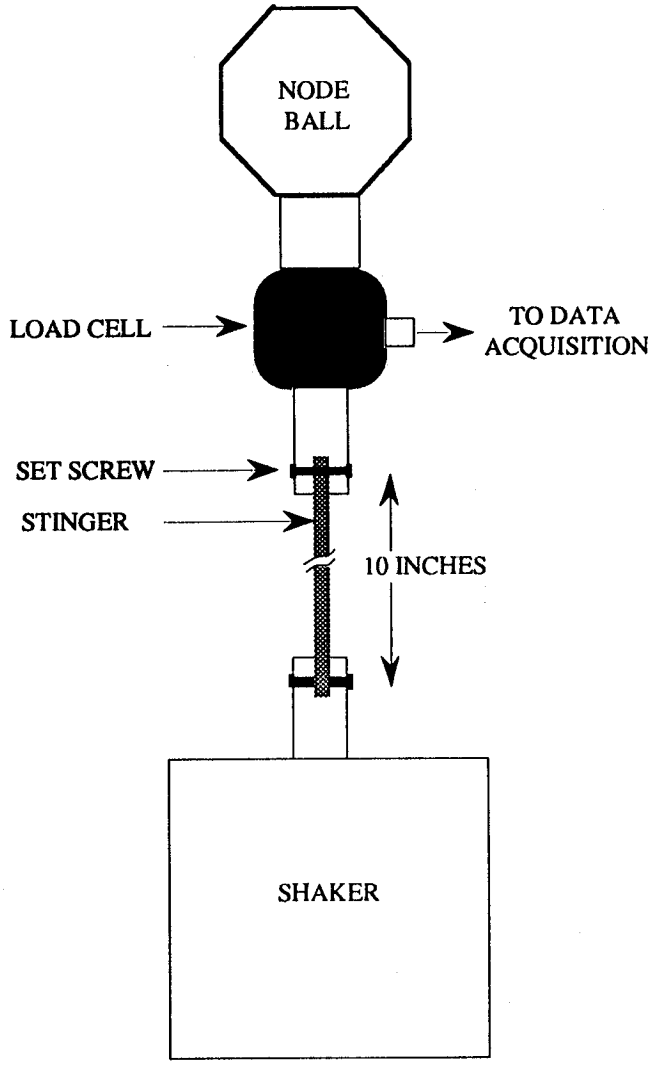

Figure 12 Stinger-load cell configuration

Sensor Placement

In the EB97-A test, three accelerometers were placed at each of the 32 un-restrained nodes of the truss to measure the accelerations in each of the x, y and z directions. In addition, one sensor was placed in the direction of the second shaker in order to provide a true driving point FRF. This was necessary because the shaker was not aligned with the global x-y-z axes. A dummy DOF was created (DOF 37Y) in the analytical model for placement of the 97th sensor. The accelerometers used were PCB Flexcels, model 336B with a frequency range of 1 - 2000 Hz and a nominal sensitivity of 1 volt / g of acceleration. Each 3-sensor and mounting block cluster had a mass of 11 grams and was

mounted on the truss using hot glue. The sensor cables were off loaded onto stands to reduce the effect of cable masses on the frequencies of the truss. Figure 13 shows the node-ball and accelerometer configuration. Figure 14 is a photograph of node 4 showing the accelerometer mounting and load cell/stinger attachment. Figure 15 shows the sensor, stinger, load cell and shaker configuration for node 7.

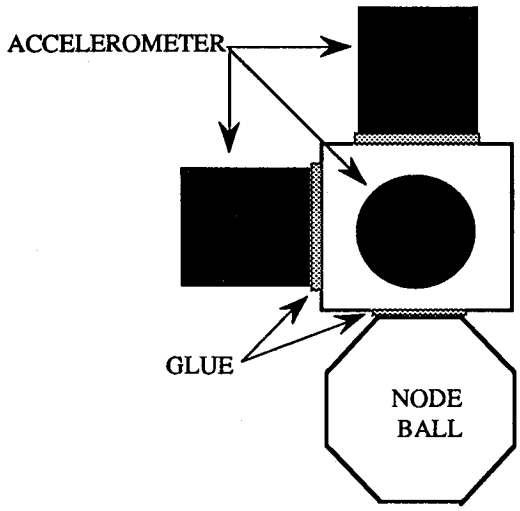

Figure 13 Accelerometer mounting

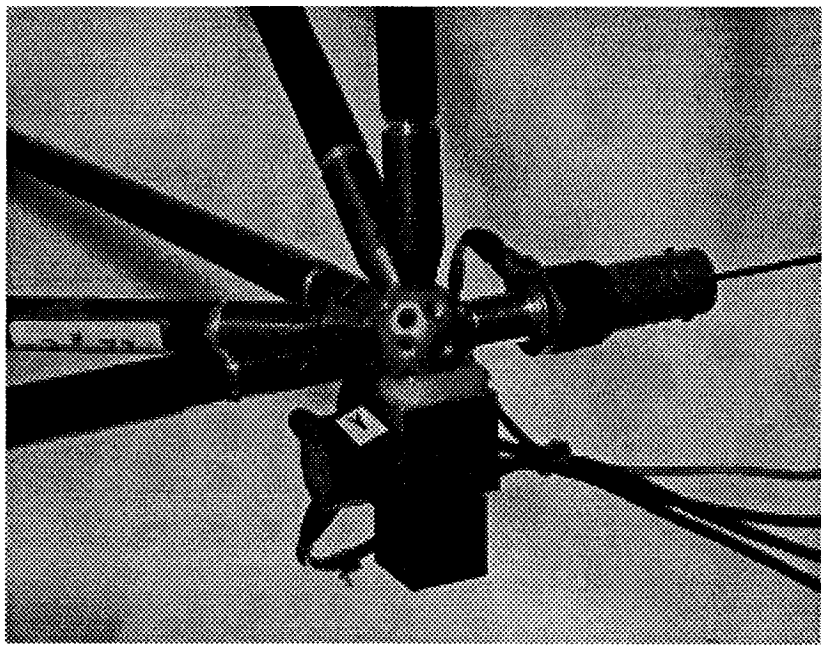

Figure 14 Eight bay instrumentation, node

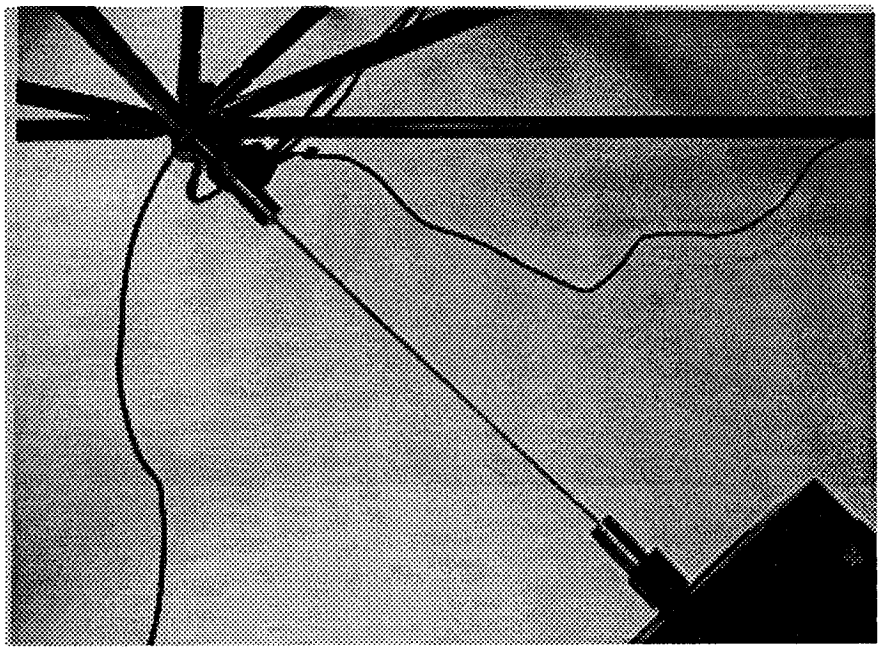

Figure 15 Eight bay instrumentation, node 7.

Data Acquisition and Test Procedures

For most of the eight bay tests, a sixteen channel GEN RAD 2515 data acquisition system was used to acquire the acceleration and force time histories and perform the preliminary signal processing on the data. With only sixteen channels of data being acquired simultaneously, the time required for a single 97 accelerometer test often exceeded five hours. Processing of the data added considerably to the overall test time. Environmental conditions can change dramatically over a period of five hours, resulting in changes in sensor calibration and possible errors in measurement. Consistency between data sets was therefore very difficult to achieve.

The EB97-A test was performed using a Zonic 7000 data acquisition system. This system is capable of handling 256 channels of input simultaneously, thus reducing the length of a single damage case test to under half an hour. Data acquisition and parameter estimation for the 16 damage cases took less than 20 hours. The quality and consistency of the data from one damage case to another is therefore considerably better than the previous tests. Frequencies, mode shapes and damping ratios for the EB97-A data are very accurate as will be described in the next section.

Following is a description of each of the steps performed in preparation for, and execution of, a typical test.

1. *Calibrate accelerometers and load cells*

   At the beginning of the testing process, each of the 97 accelerometers and the two load cells were subjected to a known input. The resulting voltage output was divided by the input to provide the actual sensor sensitivity to a unit input. The calibration constants are used in the signal processing to arrive at the amplitude and phase of the frequency response functions, and thus the mode shapes. Accurate frequencies can be obtained with poor calibration but the mode shape scaling can be severely affected if the accelerometer calibration constants are inaccurate.

   Sensor calibration could prove to be troublesome for an orbiting structure. In the lab, accelerometers are calibrated using hand-held vibrators that emit a signal at a known, constant frequency and amplitude. In space a more autonomous calibration system will have to be developed so that astronauts do not need to leave the spacecraft for the calibration process.

2. *Perform system check to verify cable connections and joint tightness.*

   With a large number of accelerometers it is easy to orient one in the wrong direction, cross wires from one sensor to another, or have loose connections. It is critical that a simple test be performed, mode shapes estimated and the directions and operation of all sensors verified. This can save considerable time on tracking errors and modifying data after the fact.

3. *Autorange data acquisition channels.*

   At the beginning of the testing process, a continuous random signal is sent to the two shakers. The response from each of the load cells and accelerometers is measured and the full scale voltage (FSV) for each of the channels adjusted so that all of the signal is within the FSV range. This FSV is then multiplied by a factor of 2 or 3 to avoid overloads during the data acquisition process.

4. *Set force levels in shakers and verify uncorrelated forces. Set block size, burst on and off duration, and number of averages.*

In the EB97-A tests the shakers were driven by a **burst random** excitation generated by the Zonic signal generator capability. Burst random excitation was selected for these tests because it tends to result in more accurate FRFs in lightly damped structures than other types of excitation. The signal generator produces a random mixture of amplitudes and phases for the entire frequency range of interest (in this case 0 to 128 Hz). A different random signal is generated and output for several successive cycles. Measurements are acquired in each cycle and averaged to produce the final FRF. Each cycle consists of a signal ON time in which the generator sends the *two different* random signals to the shakers and an OFF time in which no signal is transmitted. The total cycle time is determined by the resolution desired. The resolution is a function of how many spectral lines are used in the frequency range. This is known as the **block size**. For the EB97-A tests, a block size of 4096 was used. This results in 1600 alias free spectral lines or 32 lines per Hz. With such high resolution it is expected that the frequencies and mode shapes should be extremely accurate.

For a 4096 block size over a 128 HZ range, the total time required by the analyzer to acquire the data and store it was determined to be 12.5 seconds. By trial and error the ON time was set at 4.5 seconds and the OFF time at 8.0 seconds. This allowed the entire burst to die out while the response was being stored before the next cycle was started. 25 averages were used in each test.

For a structure such as the Space Station, the only source of excitation will be from the reaction control thruster (RCS) jets. Studies are currently underway [12] to determine ways to generate pseudo-random excitations using pulsed firings of the RCS thrusters. Due to data handling and storage considerations it is unlikely that very large block sizes will be used for on-orbit data acquisition thus limiting the resolution and accuracy of the measured modes and frequencies.

6. *Acquire data.*

Once all parameters have been set and verified, data is acquired. The signal generator sends out its first cycle and for 4.5 seconds the structure is forced to vibrate. The response from each of the channels is stored and an FFT is performed on the time history in the following 8 seconds. Once the data has been stored the signal generator triggers again, and the process is repeated. At the end of each cycle the driving point FRFs are displayed on the terminal along with the coherence function for each force signal. In addition, a display shows the status of each of the accelerometer channels and monitors the FSV to ensure that the signal remains within acceptable limits. If the signal from the sensor goes above the FSV the channel overloads and that cycle can be rejected from the averaging. Likewise, if the signal is too low (below 10% of the FSV), the cycle can be rejected. In all of the 16 cases, only one overload and no underloads occurred.

6. *Examine driving point FRF and at least one other FRF for each set to verify good data.*

Once the 25 cycles are completed and the averaging performed by the analyzer, the driving point FRFs should be examined to ensure that all of the modes of interest were excited and that the quality of the data is acceptable. The coherence function and the cross spectra should also be examined to ensure that all anomalies can be explained.

7. *Store FRFs and/or acceleration time histories.*

Depending on the parameter estimation procedure that is going to be used, either the FRF's or the time histories should be stored on the hard disk of the data acquisition system. Reference [13] presents the theory behind a number of commonly used parameter estimation techniques. In the EB97-A tests, both time histories and FRFs were stored. The parameters reported in this work were estimated using the Polyreference technique from the FRFs. However, the ERA parameter estimation method is likely to be used for orbiting structures and this method requires time histories. It is anticipated that the time histories stored from these tests will be used in ERA at a later date.

8. *Re-configure truss for next test.*

The ease of re-configuring the eight bay truss for different damage cases made the process very simple. The removed strut from one case is replaced and the next one taken out within a matter of minutes. In most cases autoranging between test cases was not performed. Once the new strut was removed, data was acquired immediately.

Data Reduction and Post-Processing

Frequency Response Functions

An FFT of the time domain data (accelerometer time histories) was performed automatically by the analyzer in the data acquisition system, transforming it to the frequency domain. Dividing by the two different inputs from the load cells gives the frequency response functions corresponding to equation (17). Several FRFs will be shown in the next section.

Parameter Estimation

The Polyreference parameter estimation technique, as implemented in the I-DEAS TDAS™ module [14], was used to extract the first five modes from each of the test cases. At frequencies higher than 75 Hz, the modes of the individual diagonals overlap with the global truss modes and identifying these global modes becomes very difficult. In some cases it was possible to obtain accurate frequencies for the sixth mode, but mode shape extraction was very inaccurate. For this reason, only results for modes one through five will be reported to maintain consistency in damage location evaluation for all cases. A detailed description of the Polyreference parameter estimation technique is beyond the scope of this work. Reference [14] has a detailed derivation and practical details for correct use of the method. Suffice it to say that the output from the Polyreference parameter estimation is a set of modal properties consisting of a mode shape coefficient at each DOF, a damping ratio for each mode and the frequency, in Hz. These modal properties are output to an I-DEAS Universal file which can be translated using a FORTRAN code into MATLAB™ readable format.

Post-Processing of Test Mode Shapes.

The mode shapes, that are the end-result of the Polyreference parameter estimation, are scaled arbitrarily and are not usually orthogonal with respect to the finite element mass matrix. In order to make them useful in the damage location and model correlation it is necessary to scale them such that they are orthogonal with respect to the FEM mass matrix. Each set of eight bay test modes $[\Psi]$, of dimension 96 x 5 (the extra DOF used for generating the driving point FRFs is not included in the final modes), was scaled to unit modal mass

$$\{\phi\}_i = \frac{\{\psi\}_i}{\sqrt{\{\psi\}_i [M] \{\psi\}_i}} \tag{18}$$

If the test data is of good quality, the cross-orthogonality matrix of the scaled modes will have unit diagonals (this will be true in all cases if equation (18) is used), and very small off-diagonal terms. If the off-diagonal terms are close to zero, no further processing of the data is usually required. If the off-diagonal terms are larger than 0.05, an optimal orthogonalization method such as those described in Reference [15], should be employed to improve the modes.

EIGHT BAY TEST RESULTS

In this section, the results for several interesting damage cases will be presented, along with comments about all of the tests results. Table 6 and Figure 16 show the test frequencies for each of the damage cases. Notice that no results are reported for mode six, as explained earlier.

Table 6 Damage Case Frequencies (From Test)

DAMAGE CASE	MODE 1	MODE 2	MODE 3	MODE 4	MODE 5
NO DAM	13.88	14.48	48.41	64.03	67.46
A	9.50	13.94	48.50	64.08	65.80
B	14.52	14.22	36.73	57.28	65.82
C	9.50	13.94	48.52	64.16	65.91
D	13.47	14.12	35.65	60.18	65.86
E	13.90	14.52	48.53	64.31	67.54
F	13.91	14.52	48.53	64.41	67.86
G	13.91	14.52	48.44	64.34	67.54
H	11.39	13.97	48.53	59.90	64.50
I	13.21	14.44	36.68	61.35	66.96
J	11.42	13.96	48.57	59.91	64.61
K	13.46	14.47	41.01	64.41	67.98
L	12.29	14.50	48.67	50.65	67.76
M	13.73	14.55	48.68	54.76	67.71
N	13.98	14.61	48.83	64.20	65.24
O	9.86	13.74	36.66	58.86	63.35
P	13.83	14.24	48.43	64.03	66.42

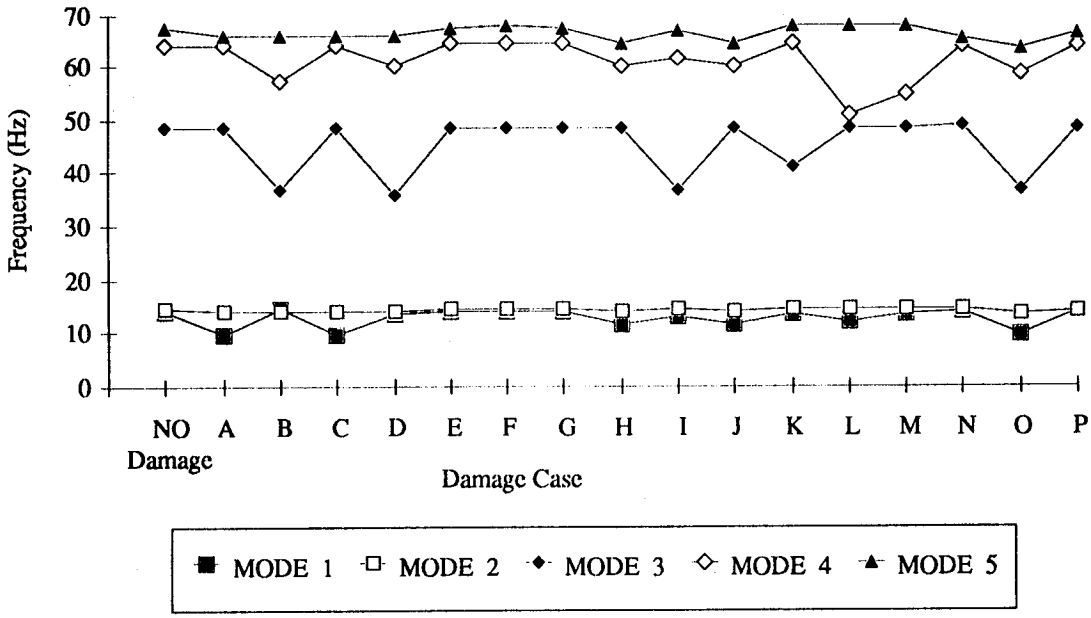

Figure 16 Frequency variations for eight bay test cases

Undamaged Truss

The first test performed was for the undamaged structure. Figure 17 shows the driving point frequency response functions for the undamaged structure. The first two modes are almost indistinguishable from each other. Recall that the frequencies for these modes from the FEM analysis were separated by only half a Hertz. One of the most critical observations that can be made from this figure is that the diagonal and longeron modes begin to interfere with the global modes above 80 Hz. This could not be anticipated from the FEM, because the FEM analysis only identifies global modes. Although it is possible in some of the damage cases to extract the sixth mode (axial) it varies considerably from test to test. For this reason, modes and frequencies for only the first five modes were estimated and used in the damage location studies.

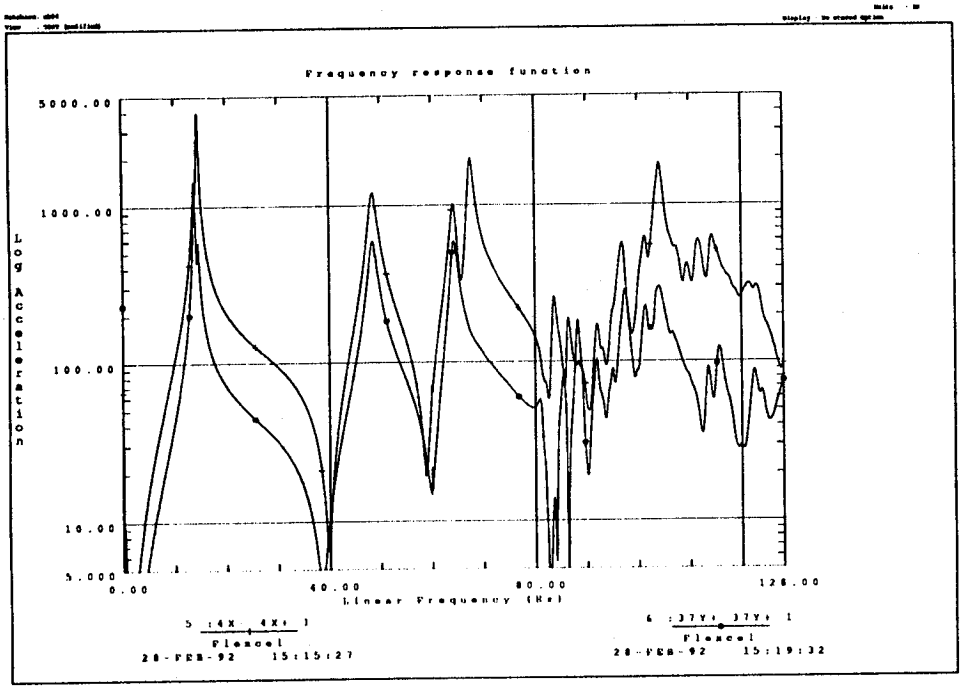

Figure 17 Driving point FRFs. Undamaged truss

Damage Case A

In damage case A, Longeron 46, in bay one was removed. This is one of the most highly strained members in the truss. Modes one and two are obviously separated considerably compared with the undamaged case and are easily distinguishable. Modes four and five are closer together. The torsional mode appears unchanged in damping and frequency, as well as amplitude. Notice, also, that many more high frequency modes appear to have been excited.

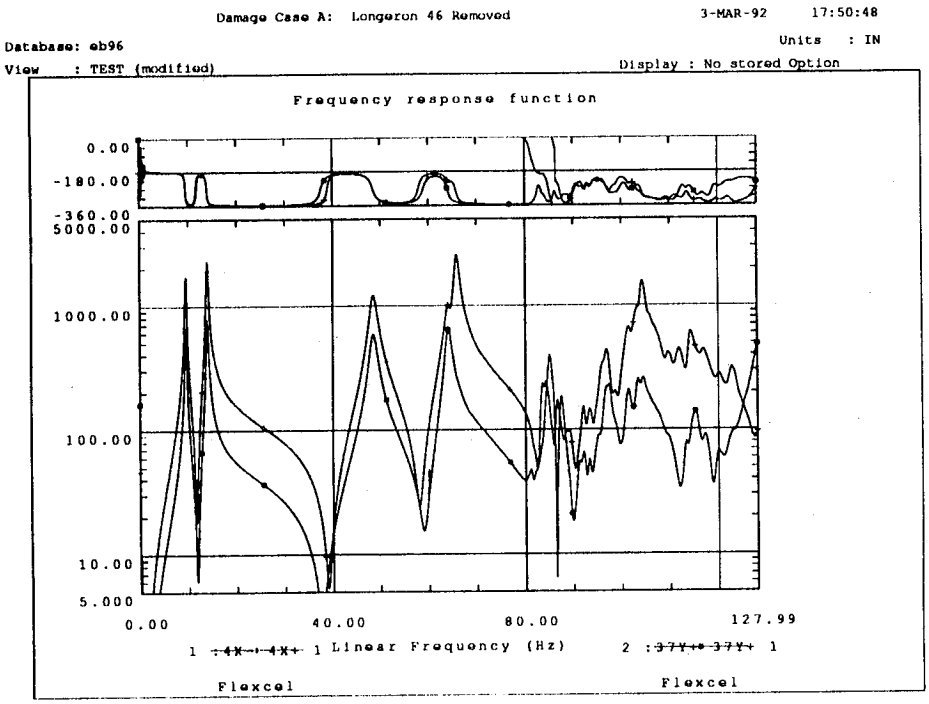

Figure 18 Driving point FRFs. Damage case A

Damage Case D

In damage case D, diagonal 102, on top of the second bay was removed. The FRFs for this case are considerably different from those from damage case A. When a diagonal is removed, the mode that is affected the most is the torsional mode. Notice that the torsional mode (mode three) has shifted considerably lower in frequency and has much lower damping than in the undamaged structure. Also notice that modes four and five have changed considerably in frequency, amplitude and perhaps order.

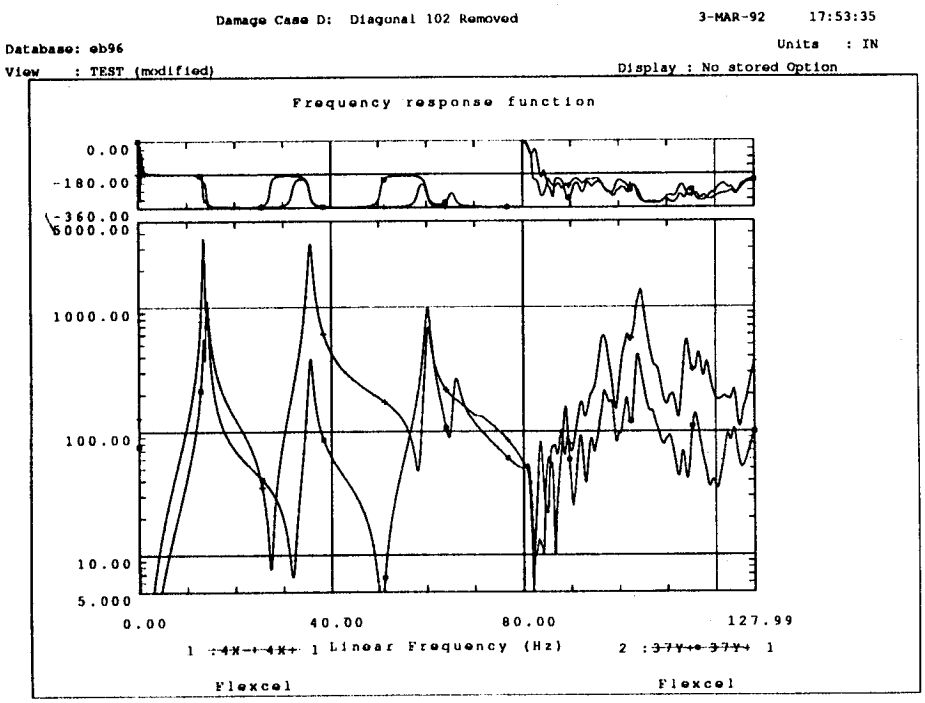

Figure 19 Driving point FRFs. Damage case D

Damage Case E

In damage case E, batten 36 in the x-direction was removed. Notice that this FRF looks almost identical to the undamaged structure. This is because the battens do not contribute significantly to the strain energy of any of the first five modes. If the axial mode had been estimated there would have been some noticeable change. If damage to this member can be located with such small changes then the damage location method is indeed very robust.

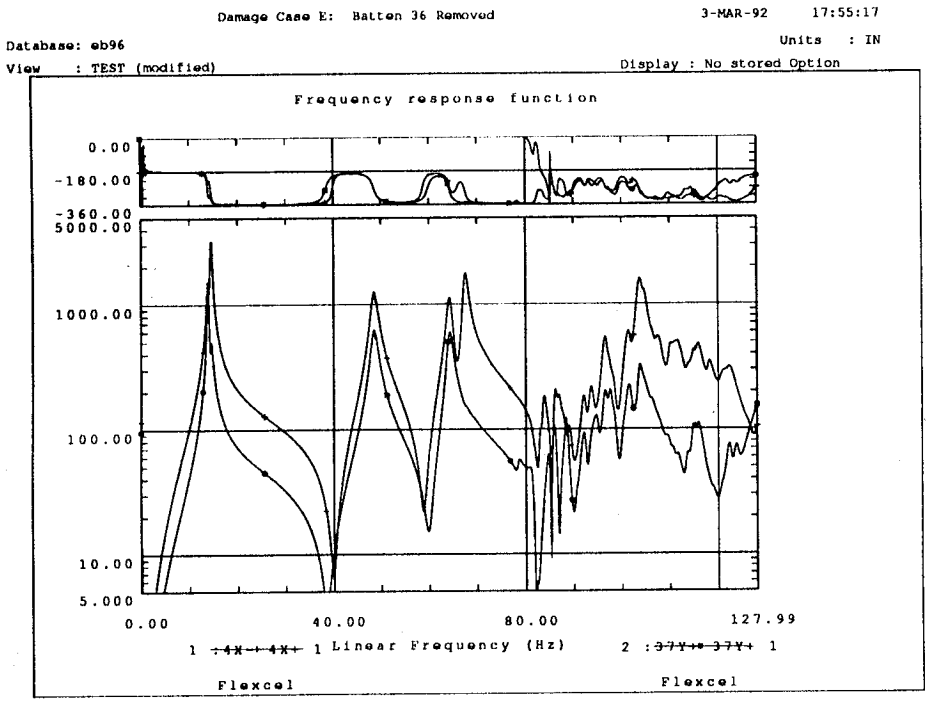

Figure 20 Driving point FRFs. Damage case E

Damage Case H

Damage case H is perhaps the most interesting of all the damage cases. This is because Longeron 35 is far enough away from the boundary to have medium contribution to the strain energy of the first two modes, but is close enough to the largest region of curvature to have a higher contribution in the second bending mode pair. Notice that the distance between modes one and two is large, but not as large as in damage case A. Also notice the distance between modes four and five, and the fact that the lower FRF picks up mode five clearly, but not mode four, a reversal from the undamaged FRFs and a good indication that the modes may have switched order..

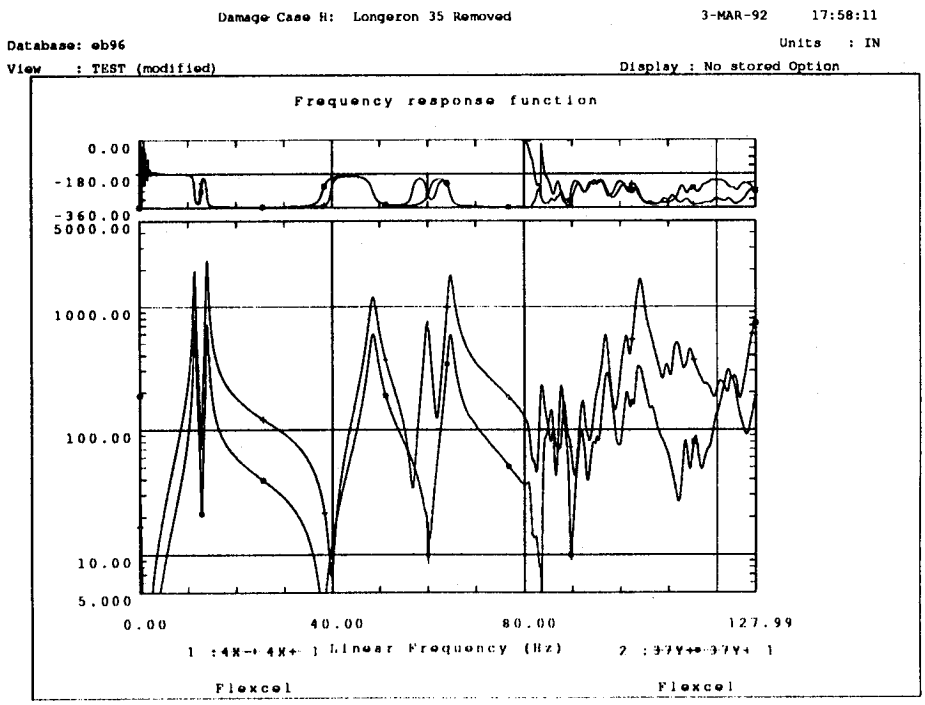

Figure 21 Driving point FRFs. Damage case H

Damage Case J

Damage case J is interesting for a very important reason. When Longeron 28 is removed, Mode 4 is changed such that the frequency is exactly 60Hz. All electrical power in the lab operates near 60Hz. The 60Hz mode of the damage structure is therefore interfered with considerably. Figure 22 is an enlargement of the 60 Hz mode showing this interference. The polyreference estimate of the frequency for this mode is inaccurate because it is unable to resolve the peak.

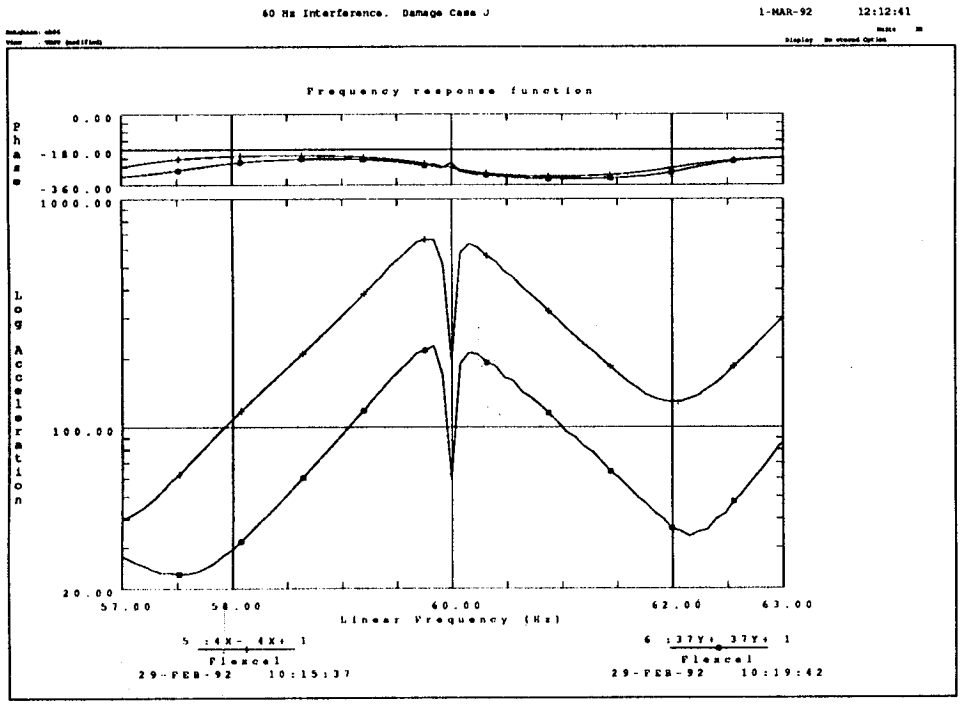

Figure 22 60 Hz interference. Damage case J

Damage Case P

In damage case P a longeron that had buckled during static testing, was inserted in the place of longeron 35. The member was visibly bent and it was anticipated that the load carrying capacity would be diminished. The FRF, however, appears identical to the undamaged FRF.

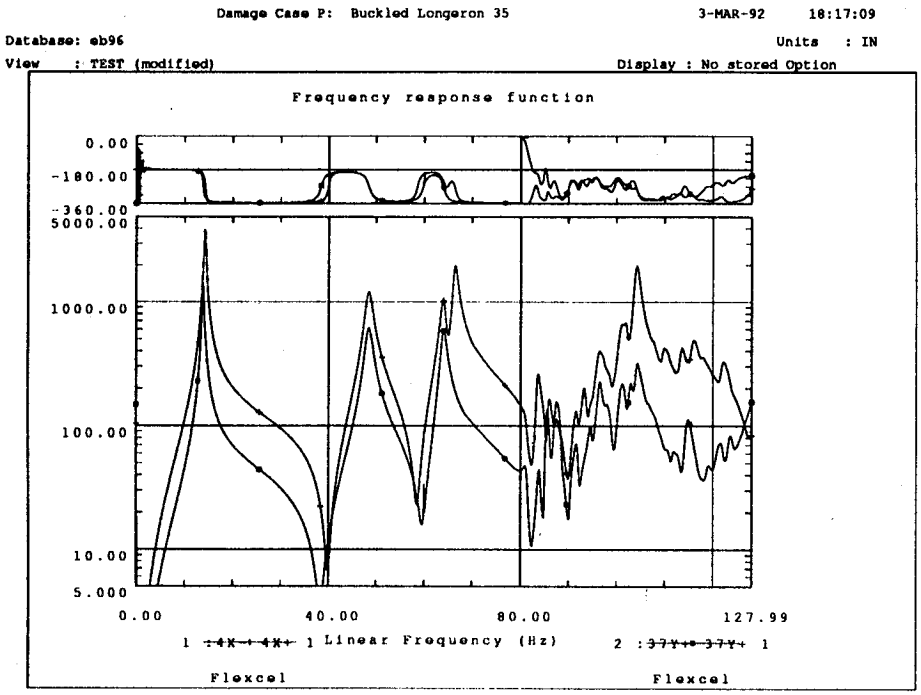

Figure 23 Driving point FRFs. Damage case P

Each of the driving point FRFs from the other damage cases was also examined in detail before modal parameters were estimated.

CORRELATION OF TEST DATA WITH FINITE ELEMENT PREDICTIONS.

The results from the 14 single member tests and the one multiple member test were correlated with those from the corresponding finite element analyses. Percent differences between the frequencies are shown in Figure 24. Notice that , with a few exceptions, the frequencies are correlated to within ± 5%. The discrepancies could be from errors in the test data or errors in the finite element model. No effort was made to determine the cause of the discrepancies. It should be noted that the finite element model was not modified in any way based on this test data and as such can be considered a *first generation finite element model.* Model Refinement and Damage Location researchers can use their methods to modify the finite element model using the results of the undamaged truss test and then attempt to locate damage using the remainder of the test data. Mode shapes were also correlated with similar results.

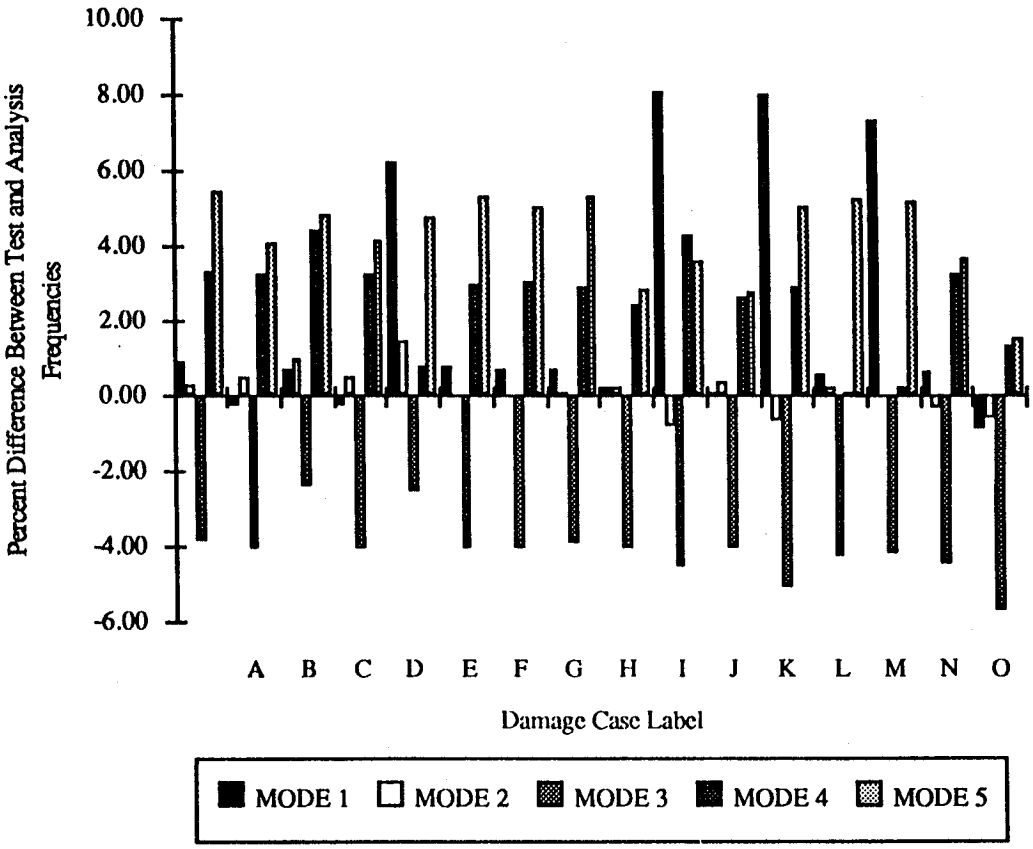

Figure 24 Test/Analysis Frequency Correlation

SUMMARY

A detailed description of a laboratory truss structure has been presented in this report. In addition, details of the design of the tests that were performed to study damage location were described. A brief summary of modal testing theory is included for completeness. A step by step description of the procedures used during testing precedes documentation and description of some of the results and trends that can be deduced from these results.

The test article is an eight bay section of truss that is one tenth the size and has five times the dynamics of an early concept of the Space Station Freedom truss. The truss was subjected to a series of modal tests from which modes and frequencies were extracted. Frequency response functions from the tests are presented to demonstrate the quality of the data that can be expected from such tests. Differences between the process of acquiring modal parameters from a ground vibration test and an on-orbit modal test are discussed.

The tests presented here and the data collected constitute a significant contribution to the field of damage detection. The data is available to other researchers and will be used as a benchmark for development and verification of new model refinement and damage location techniques.

REFERENCES

1. Kashangaki, T., "Damage Location and Model Refinement for Large Flexible Space Structures Using a Sensitivity Based Eigenstructure Assignment Method," Ph.D Dissertation, University of Michigan, May 1992.

2. Smith, S.W., and Hendricks, S.L., "Damage Detection and Location in Large Space Trusses," AIAA SDM Issues of the International Space Station, A Collection of Technical Papers, Williamsburg, Virginia, April 21-22, 1988, pp. 56-63.

3. Lim, T.W., "Analytical Model Improvement Using Measured Modes and Submatrices," *AIAA Journal*, Vol. 29, No. 6, June 1991, pp. 1015-1018.

4. Zimmerman , D.C., and Kaouk, M., "Structural Damage Detection Using a Subspace Rotation Algorithm," 33rd AIAA SDM Conference, Dallas, TX, April 13-15, 1992.

5. Smith, S. W., and McGowan, P.E., "Locating Damaged Members in a Truss Structure Using Modal Data: A Demonstration Experiment," NASA TM-101595, April 1989.

6. MSC/NASTRAN User's Manual. Version 66. The Macneal-Schwendler Corporation. 1989.

7. I-DEAS Finite Element Modeling User's Guide, Structural Dynamics Research Corporation, 1990.

8. Ewins, D.J., Modal Testing: Theory and Practice. Research Studies Press, 1984.

9. MATLAB™ User's Guide, The MathWorks, Inc., 1991.

10. Kashangaki, T., "On-Orbit Damage Detection and Health Monitoring of Large Space Trusses - Status and Critical Issues," Proceedings of the 32nd AIAA SDM Conference, Baltimore, MD, April 8-10, 1991. Also published as NASA TM-104045.

11. Kashangaki, T. , Smith, S. W., and Lim, T.W," Underlying Modal Data Issues for Detecting Damage in Truss Structures, " For Presentation at the 33rd AIAA SDM Conference, Dallas, TX, April 13-15, 1992.

12. Cooper, P.A., and Johnson, J.W.," Space Station Freedom On-Orbit Modal Identification Experiment- An Update", 2nd USAF/NASA Workshop on System ID and Health Monitoring of Precision Space Structures, Pasadena, CA. March 1990.

13. Juang, J., "Mathematical Correlation of Modal-Parameter-Identification Methods Via System Realization Theory, "*International Journal of Analytical and Experimental Modal Analysis*," Vol. 2, No. 1, January 1987, pp. 1-18.

14. I-DEAS Test Data Analysis User's Guide, Structural Dynamics Research Corporation, 1990.

15. Smith, S.W., and Beattie, C.A., "Simultaneous Expansion and Orthogonalization of Measured Modes for Structure Identification", Proceedings of the AIAA SDM Dynamics Specialist Conference, Long Beach, California, April 5-6, 1990, pp. 261-270.

REPORT DOCUMENTATION PAGE

Form Approved
OMB No. 0704-0188

1. AGENCY USE ONLY (Leave blank)	2. REPORT DATE	3. REPORT TYPE AND DATES COVERED
	May 1992	Technical Memorandum

4. TITLE AND SUBTITLE
Ground Vibration Tests of a High Fidelity Truss for Verification of On Orbit Damage Location Techniques

5. FUNDING NUMBERS
WU 590-14-31-01

6. AUTHOR(S)
Thomas A. L. Kashangaki

7. PERFORMING ORGANIZATION NAME(S) AND ADDRESS(ES)
NASA Langley Research Center
Hampton, VA 23665-5225

8. PERFORMING ORGANIZATION REPORT NUMBER

9. SPONSORING/MONITORING AGENCY NAME(S) AND ADDRESS(ES)
National Aeronautics and Space Administration
Washington, DC 20546-0001

10. SPONSORING/MONITORING AGENCY REPORT NUMBER
NASA TM-107626

11. SUPPLEMENTARY NOTES
Thomas A. L. Kashangaki: Langley Research Center, Hampton, VA
Compilation of data used in AIAA paper #92-2264 presented at the 33rd Structures, Structural Dynamics & Materials Conference, Dallas, TX, April 13-15, 1992

12a. DISTRIBUTION/AVAILABILITY STATEMENT
Unclassified--Unlimited

Subject Category 39

12b. DISTRIBUTION CODE

13. ABSTRACT *(Maximum 200 words)*

This paper describes a series of modal tests that were performed on a cantilevered truss structure. The goal of the tests was to assemble a large database of high quality modal test data for use in verification of proposed methods for on orbit model verification and damage detection in flexible truss structures. A description of the hardware is provided along with details of the experimental setup and procedures for sixteen damage cases. Results from selected cases are presented and discussed. Differences between ground vibration testing and on orbit modal testing are also described.

14. SUBJECT TERMS
Modal Testing, Damage Location, On Orbit Verification, Dynamics of Large Flexible Space Structures

15. NUMBER OF PAGES
38

16. PRICE CODE
A03

17. SECURITY CLASSIFICATION OF REPORT	18. SECURITY CLASSIFICATION OF THIS PAGE	19. SECURITY CLASSIFICATION OF ABSTRACT	20. LIMITATION OF ABSTRACT
Unclassified	Unclassified		